Disorder-driven two-dimensional quantum phase transitions in Li x MoS 2

Ivan Verzhbitskiy, Damien Voiry, Manish Chhowalla, Goki Eda

2D Materials

Disorder-driven two-dimensional quantum phase transitions in Li_xMoS₂

To cite this article before publication: Ivan Verzhbitskiy *et al* 2020 *2D Mater.* in press https://doi.org/10.1088/2053-1583/ab8690

Disorder-driven two-dimensional quantum phase transitions in Li_xMoS_2

Ivan A. Verzhbitskiy,[1,2,*] Damien Voiry,[3] Manish Chhowalla,[4] and Goki Eda[1,2,5,*]

[1]Department of Physics, National University of Singapore, Singapore
[2]Centre for Advanced 2D Materials, National University of Singapore, Singapore
[3]Institut Européen des Membranes, Université de Montpellier, France
[4]Department of Materials Science & Metallurgy, Cambridge University, UK
[5]Department of Chemistry, National University of Singapore, Singapore
[*]Correspondence to: ivan@nus.edu.sg; g.eda@nus.edu.sg

Quantum phase transition (QPT) is the keystone in understanding the quantum state of matter. Here we report observation of QPT and its evolution in nanosheets of Li_xMoS_2 with various degrees of disorder introduced by progressive thermal annealing. The material exhibits onset of superconducting transition at temperatures ranging between 3 and 6 K. We show that the angular dependence of the upper critical field is well described by Tinkham's (2D) model. Finite-size scaling analysis reveals that the pristine samples with predominantly T/T' phases exhibit magnetic-field driven superconductor-to-metal QPT. We further show that annealed samples with a higher content of 2H phase exhibit QPT with diverging critical exponents similar to the recently reported behaviours of highly crystalline 2D superconductors.

Introduction

Disorder plays a fundamental role in defining the nature of superconducting transition in low-dimensional systems [1, 2]. In the past decades, thin films of amorphous metals such as Bi [3] and MoGe [4] were the main model systems to study the effect of disorder for 2D superconductors. The degree of disorder in these systems can be controlled by deposition and processing conditions, allowing destruction of superconductivity to be studied systematically. Superconductor-insulator transition (SIT) in these films are believed to be purely driven by quantum fluctuations at T = 0 K. Recently, such quantum phase transition (QPT) has been reported in 2D superconductors based on crystalline van der Waals layered materials [5], opening up studies of various exotic phenomena, such as quantum metal ground state [6], Ising superconductivity [7-9] and Griffiths singularity [10, 11]. However, unlike the traditional amorphous metals and recent ultrathin crystalline films such as Ga [12], Pb [13, 14] and

$YBa_2Cu_3O_{7-x}$ (YBCO) [15], the effect of disorder in these van der Waals layered superconductors has not been studied systematically due to lack of controlled approach to introducing disorder.

Intercalation compounds of transition metal dichalcogenides are potentially an ideal platform to study the effects of disorder on 2D superconductivity due to their versatile chemistry [16, 17]. Superconductivity in intercalation compounds of MoS_2 have been extensively studied in the 70's and 80's. They superconduct below a critical temperature T_c of 3~7 K depending on the guest species and their concentration [18-20]. It is known that A_xMoS_2 (where A represents the intercalating species) often contain inherent disorder due to coexistence of multiple structural phases [21]. Recently, potassium intercalated compound, K_xMoS_2, was found [22] to exhibit anomalous changes in the magnetic susceptibility as a function of temperature, which were attributed to the coexistence of three crystalline phases: 1T, 1T', and 2H, all of which are well-known polymorphs of MoS_2. The composition of the structural phases depends on the concentration of intercalating species [23]. Fully intercalated A_xMoS_2 with $x\approx1$ consists primarily of metallic T/T' phases whereas at lower values of x, the semiconducting 2H phase coexists with the T/T' phases. Thus, A_xMoS_2 represents a unique 2D crystalline superconducting platform in which the degree of quenched disorder can be continuously varied via either intercalation or de-intercalation.

Here, we report the onset of superconducting transition in exfoliated nanosheets of Li_xMoS_2 having different structural phase compositions prepared by annealing-induced phase changes. We show that the pristine crystals with a high content of T/T' phases exhibit magnetic-field-driven SIT that can be described as a 2D QPT phenomenon. With increased disorder induced by mild annealing resulting in reduction of the superconducting phase, we observe modification to the scaling behaviors of QPT. We propose possible formation of rare

superconducting islands, similar to the cases of recently reported ultrathin crystalline films [10-13, 15].

Results

Lithium-intercalated MoS_2 single crystals (Fig. 1a) were directly synthesized by chemical vapor transport (CVT). In contrast to MoS_2 intercalated using butyllithium, we found that direct growth of Li_xMoS_2 yields high quality crystals with a high concentration of T/T' phases. We identified T/T' polymorphs of MoS_2 using electron microscopy, X-ray photoemission (XPS) and Raman spectroscopy. Based on XPS analysis, we estimate the T/T' phase content to be >80% in pristine crystals (Fig. S1). Magneto-transport properties of mechanically exfoliated Li_xMoS_2 crystals (from 4 to 40 nm in thickness) were studied on SiO_2/Si substrates after fabricating multi-terminal devices by standard e-beam lithography and thermal evaporation of metal contacts (Fig. 1b). From Hall measurements we estimated the carrier density to be of the order of 2×10^{15} cm^{-2}. Room temperature sheet resistance of the devices was found to vary between 200 Ω and 5 kΩ. Due to moisture sensitivity of Li_xMoS_2, its exposure to air was minimized during device fabrication. Extended annealing was also avoided to prevent undesirable phase changes. While some degree of deintercalation and phase changes is unavoidable, interestingly, as-prepared devices consistently exhibited increasing resistance with temperature as expected from the metallic character of T/T' MoS_2. At temperatures ranging between 3 ~ 6 K, abrupt change in resistance was observed, indicating an onset of superconducting transition, as shown in Fig. 1b. Zero-resistance state was not observed within the temperature window of the current study, suggesting that non-superconducting phases are present in the as-prepared samples.

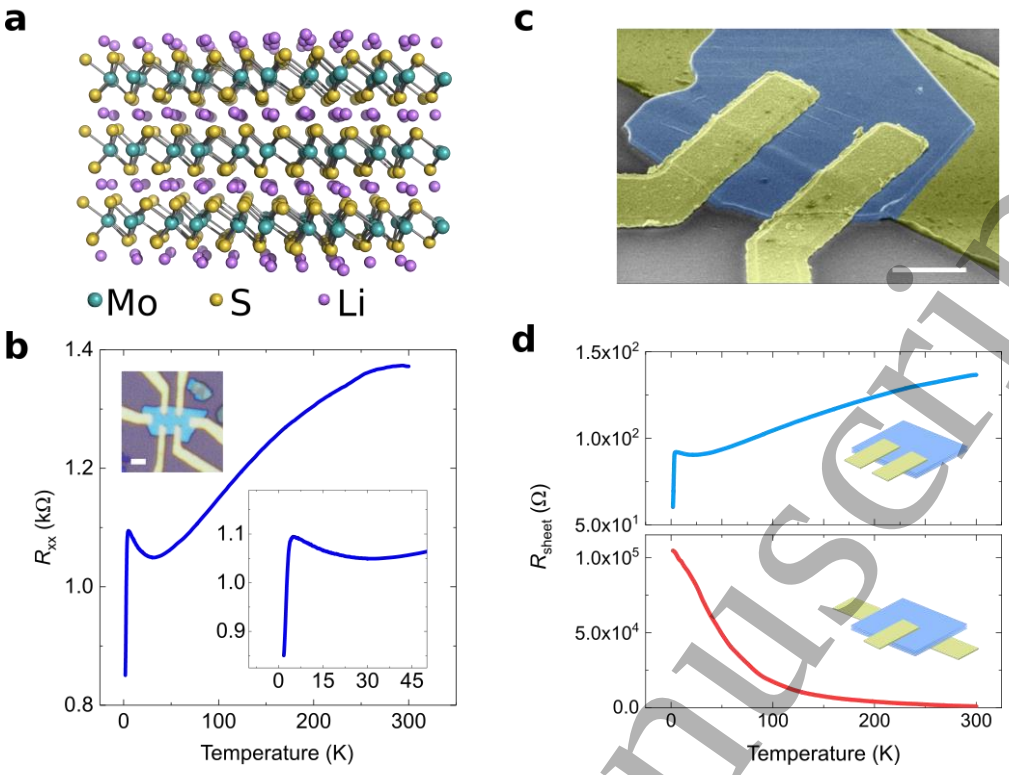

Figure 1. Characterization of Li_xMoS_2 flakes. (a) A ball-and-stick model representation of Li_xMoS_2 crystal. (b) Typical *R* -*T* dependence of a Li_xMoS_2 device. The upper inset shows the optical image of the device (scale bar is 2 μm). The lower inset shows the low-temperature region, highlighting the onset of superconductivity at the T_{onset} = 4.8 K. (c) False-colour SEM image of the device for the out-of-plane transport measurements. (d) In-plane (top panel) and out-of- plane (bottom panel) *R*-*T* curves. Insets show the measurement geometries.

We studied the conductivity anisotropy of the sample by measuring the in-plane and out-of-plane resistance of a 30 nm thick pristine Li_xMoS_2 nanosheet in two probe configuration (Fig. 1c). Figure 1d shows the contrasting temperature dependence of the in-plane and out-of-plane resistances. The out-of-plane resistance is 2~3 orders of magnitude greater than the in-plane resistance and exhibits characteristics of a band insulator with no sign of superconducting transition at low temperatures. This large anisotropy implies that superconductivity of individual layers is decoupled from each other, suggesting its 2D nature.

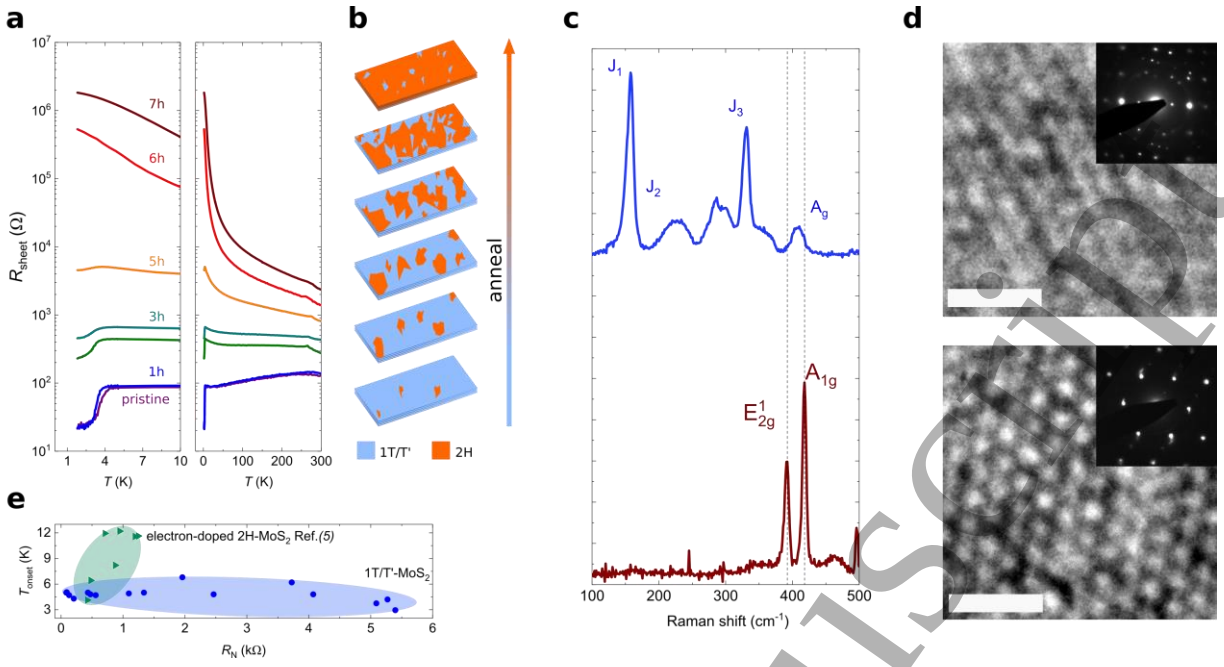

Figure 2. **Annealing of Li_xMoS_2 samples.** (a) *R-T* curves of pristine Li_xMoS_2 flake after a period of annealing. After 6 hours of annealing, the onset of superconductivity can no longer be observed under our experimental conditions. (b) Schematic represents evolution of the composition of the superconducting 1T/T' and insulating 2H phases. (c) The first-order Raman spectrum of pristine (top) and annealed (bottom) samples, respectively. (d) High-resolution TEM images if pristine (top) and annealed (bottom) samples, respectively (scale bar is 1 nm). The insets show the SAED patterns from these samples. (e) Dependence of superconductivity onset, T_{onset} on normal state resistance R_N. Green triangles represent electron-doped 2H-phase of MoS_2 (data were extracted from [5]) and blue circles represent Li_xMoS_2 samples.

In order to induce changes in phase composition, we progressively annealed the superconducting samples in steps at 100 °C in vacuum. The sample becomes a simple band insulator after prolonged annealing (Fig. 2a). However, the onset of superconducting transition is still observable for short annealing times (< 5 hrs), indicating that the restoration of the insulating phase is a gradual process as schematically illustrated in Fig. 2b. Figure 2e shows superconductivity onset temperature, T_{onset}, as a function of normal state resistance, R_N (the resistance plateau immediately above T_{onset}) for progressively annealed device as well as as-fabricated devices. It can be seen that T_{onset} remains nearly constant despite the large variation in R_N. This behavior is distinct from that of gate-induced superconductivity in 2H-MoS_2 where T_{onset} changes between 4 and 12 K when R_N changes by a factor of two at different gate biases (Fig. 2e, green symbols) [5]. This implies that the superconductivity of our samples is governed

by the 1T/T' phases rather than the heavily doped 2H phase. In other words, annealing primarily induces reduction in the superconducting phase content rather than changes in its properties due to reduction in the doping density. Thus R_N can be taken as a measure of the degree of disorder associated with the mixed phase structure. As-fabricated devices exhibit a range of R_N, suggesting that the phase composition varies across different pristine crystals. It is worth noting that T_{onset} being independent of R_N is qualitatively different from the behavior of amorphous metal films where disorder weakens Coulomb screening, reducing critical temperature [24]. However, the observed trend is similar to that of the 2D high-temperature superconductor [15] where disorder was systematically introduced and disorder-induced QPT was observed. Our observation suggests that the strength of the superconducting pairing in T/T' phase is only weakly dependent on the phase composition.

After annealing at 100 °C in vacuum for more than 5 hours, the sample relaxed to the semiconducting 2H phase as evidenced by the disappearance of the J phonon peaks of the T/T' phase and emergence of characteristic Raman A_{1g} and E_{2g} peaks (Fig. 2c). This phase relaxation is most likely accompanied by de-intercalation of lithium. The TEM images and selected area electron diffraction patterns shown in Fig. 2d show that the samples remain crystalline after annealing. The reduction in the T/T' phase content is most pronounced during the initial 1~2 hours of annealing as previously reported [25].

Discussion

2D superconductivity in pristine Li_xMoS_2

Figure 3a shows the disappearance of the superconducting transition with increasing out-of-pane magnetic field for the pristine T/T' samples. With increasing field, the sheet resistance becomes weakly temperature dependent, saturating at ~ 210 Ω at T = 2 K, which is

a behavior common to weakly localized metals. Note that this saturation resistance is well below quantum resistance ($h/4e^2$ = 6.45 kΩ) and there is no sign of insulating phase emerging in our experimental window. This trend is characteristic of magnetic-field-induced superconductor-metal transition (SMT) [26]. Strong anisotropy of the superconductivity is evident from the significantly larger in-plane magnetic field needed to destroy the superconducting phase (Fig. 3b). The dependence of the upper critical field B_{c2} (defined as the field required to reach $0.9R_N$) with temperature can be well described by the Werthamer-Helfand-Hohenberg (WHH) model, which depicts the behavior of conventional type-II superconductors (Fig. 3c) [27, 28]. The onset of superconductivity B_{onset} (defined as the field at which $\partial R/\partial T$ first changes its sign with increasing temperature) exhibits similar dependence with temperature as B_{c2}. It is worth noting, that parallel critical field curve also accurately follows the 2D Ginzburg-Landau behavior (2D-GL, $B_{c2}^{||} \sim \sqrt{1 - T/T_c}$) often used to describe the 2D superconducting systems [29]. Interestingly, within the experimental range the curve exceeds the Pauli limit (~6 T), which suggests the strong influence of spin-orbit interaction effects [30].

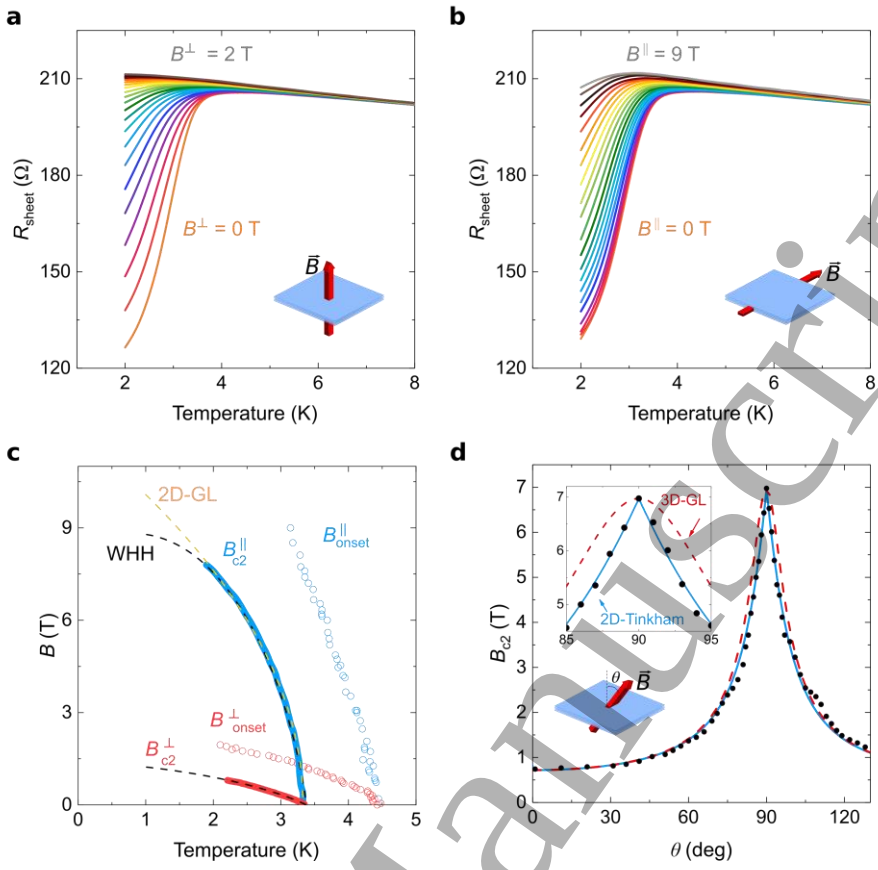

Figure 3. **2D superconductivity of pristine Li_xMoS_2.** (a,b) *R-T* dependence at a constant magnetic field (a) perpendicular and (b) parallel to the crystal layer plane. (c) The upper critical magnetic field B_{c2} (solid lines) and onset of superconductivity B_{onset} (open symbols) as a function of temperature for both parallel (blue) and perpendicular (red) directions. The curves are fitted with WHH model (black dash) and 2D-GL (orange dash). (d) Angular dependence of the upper critical magnetic field at 1.8 K. The experimental data (black) are fitted with 3D Ginzburg-Landau (3D-GL) and 2D Tinkham's model. Inset shows the feature around the peak.

From B_{c2}–*T* dependence we estimated the Ginzburg-Landau (GL) coherence length limits to be $\xi_{ab} \approx 15.5$ nm and $\xi_c \approx 2.3$ nm. Although these values are greater than the thickness of the individual MoS_2 layer (~0.7 nm), the strong anisotropy in GL coherence lengths is consistent with 2D superconductivity. Similar anisotropy has been recently observed in 2H-MoS_2 Ising superconductors [7, 8]. Our out-of-plane transport measurements further support the observation of 2D superconductivity (Fig.1d).

To further verify the dimensionality of the superconductivity, we measured the dependence of B_{c2} critical field on the angle θ between field direction and *c*-axis of the Li_xMoS_2

crystal (Fig. 3d). The angular dependence is well described by Tinkham's (2D) model ($H_{c2}(\theta)\sin\theta / H_{c2}^{\parallel} + \left|H_{c2}(\theta)\cos\theta / H_{c2}^{\perp}\right| = 1$) [31] rather than with 3D GL anisotropic mass model ($\left(H_{c2}(\theta)\sin\theta / H_{c2}^{\parallel}\right)^2 + \left(H_{c2}(\theta)\cos\theta / H_{c2}^{\perp}\right)^2 = 1$). The cusp-like feature agreeing well with the 2D model is a hallmark of interfacial superconductivity [32, 33]. These findings collaborate with the Berezinskii-Kosterlitz-Thouless [34] transition recently observed in 1T-MoS_2 [35].

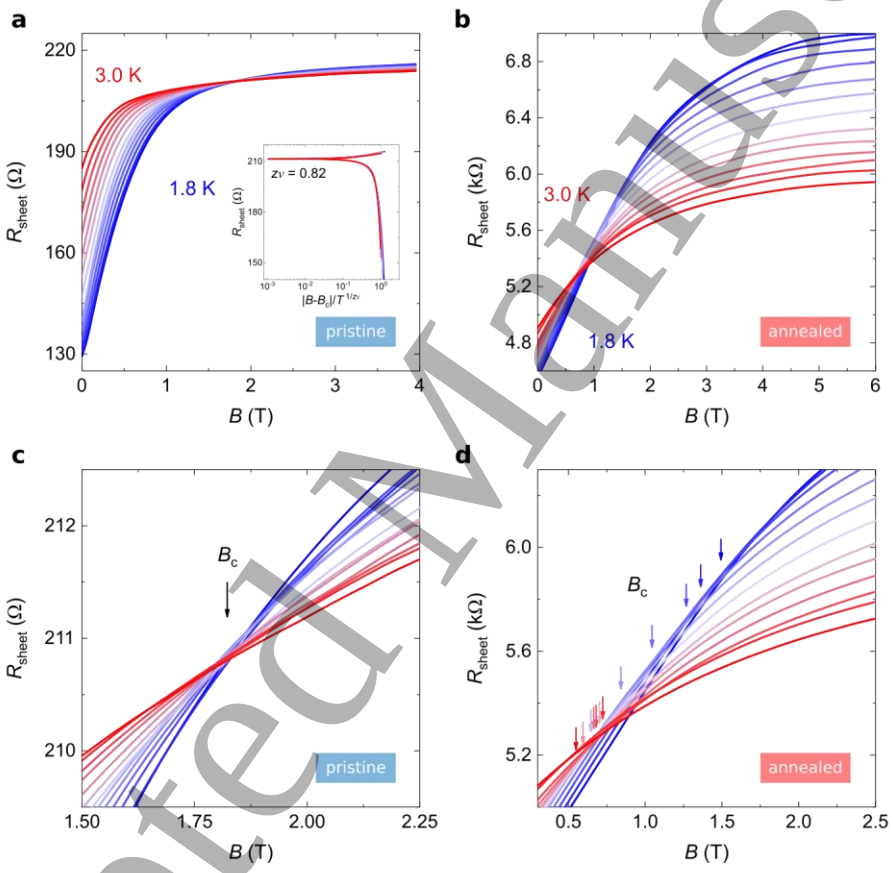

Figure 4. ***R-B* crossings for pristine and annealed samples**. Magnetoresistance isotherms in the temperature range of 1:8 - 3:0 K for pristine (a, c) and annealed (b, d) samples in different scales. The arrows in (c, d) indicate the crossing points of the adjacent isotherms. Inset in (a) shows the finite-size scaling (FSS) analysis for the isotherms of the pristine sample.

Quantum phase transition

Figure 4 shows the magnetoresistance isotherms of pristine and annealed crystal. The isotherms exhibit qualitatively different critical transition behaviors for the two samples. For the pristine sample, the low temperature curves (1.8 ~ 2.4 K) virtually cross at a single point whereas the crossing points shift systematically with temperature for the annealed sample. The single crossing behavior, which is characterized by temperature-independent critical resistance and field, is one of the key signatures of QPT. Here, we apply the finite-size scaling (FSS) analysis [36, 37], which in two dimensions has the form:

$$R(x,T) = R_c\, f\left(|x - x_c| T^{-1/z\nu}\right),$$

where x is the tuning parameter for the transition (here, perpendicular magnetic field), R_c is the critical resistance that separates the superconducting and metallic states at $x = x_c$, ν and z are the correlation length and dynamical critical exponent of QPT. Inset of the Fig. 4a shows that all the low temperature isotherms (1.8 ~ 2.4 K) collapse into a single curve, demonstrating good agreement to the above equation. The 'effective' critical exponent $z\nu$ was evaluated by taking the slope of $\log\left(\partial R/\partial B|_{B_c}\right)$ versus $\log\left(T^{-1}\right)$. For most of our pristine samples $z\nu$ values were found to be 0.7-0.8 (see Supplementary Table S1 for the summary of values obtained for 5 pristine samples).

Interestingly, the isotherm crossing behaviors of the annealed sample (Fig. 4b, d) resemble those of ionically gated ZrNCl and 2H-MoS_2 [10] which were reported to exhibit quantum Griffiths state [12]. Here we examine the isotherms of the annealed sample by performing FSS analysis for adjacent curves. Figure 5 shows the $z\nu$ values as a function of the magnetic field. It can be seen that $z\nu$ diverges towards a certain field, following activated scaling law, similar to the case of ionically gated ZrNCl and 2H-MoS_2. All annealed and some as-fabricated devices with high R_N exhibited the same behavior (Fig. 5). This diverging exponent is indicative of presence of quantum Griffiths phase, which is characterized by the

formation of weakly coupled rare superconducting regions in a non-superconducting matrix. The contrasting behaviors of as-fabricated and annealed devices suggest the role of disorder in modifying the superconducting ground state of the system.

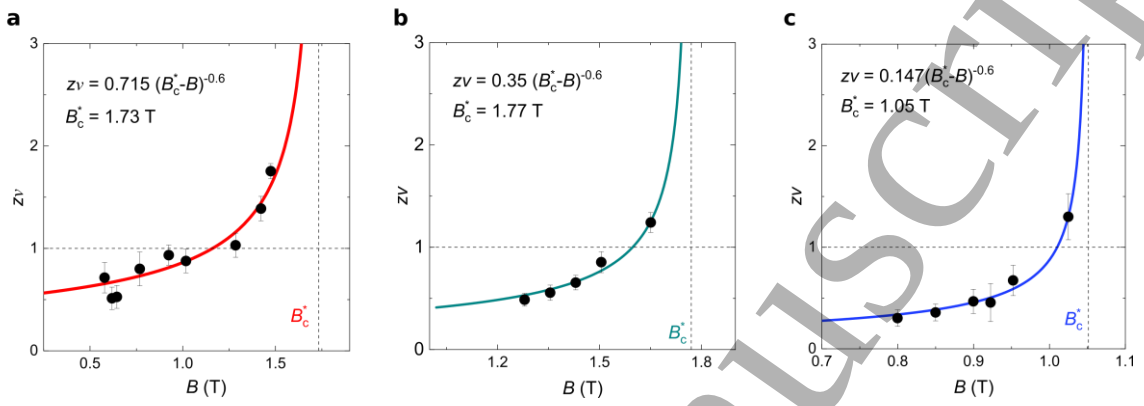

Figure 5. Quantum Phase Transition in Li_xMoS_2. Activated behaviour of the critical exponent as a function of magnetic field for annealed (a) and pristine (b, c) samples. Each value was extracted by FSS analysis. Vertical and horizontal lines represent =1.73 T and =1.

In summary, we studied the impact of mixed-phase structure of Li_xMoS_2 on its superconducting transitions. The pristine samples with a low degree of disorder consistently exhibit signatures of 2D superconductor-metal QPT. In mildly annealed samples with a higher content of 2H phase, we find that the QPT was strongly altered and exhibited scaling behaviors characterized by the diverging critical exponents, resembling the case of ionically gated ZrNCl and MoS_2. Our findings demonstrate that Li_xMoS_2 offers a versatile platform for studying non-conventional QPT due to its high crystallinity and continuously tunable disorder.

Bibliography

1. Lin, Y.-H., J. Nelson, and A.M. Goldman, *Superconductivity of very thin films: The superconductor–insulator transition.* Physica C: Superconductivity and its Applications, 2015. **514**: p. 130-141.
2. Dobrosavljevic, V., N. Trivedi, and J.M.J. Valles, *Conductor-Insulator Quantum Phase Transitions*. 2012, Oxford: Oxford University Press.
3. Haviland, D.B., Y. Liu, and A.M. Goldman, *Onset of superconductivity in the two-dimensional limit.* Physical Review Letters, 1989. **62**(18): p. 2180-2183.
4. Yazdani, A. and A. Kapitulnik, *Superconducting-Insulating Transition in Two-Dimensional a-MoGe Thin Films.* Physical Review Letters, 1995. **74**(15): p. 3037-3040.
5. Ye, J.T., et al., *Superconducting Dome in a Gate-Tuned Band Insulator.* Science, 2012. **338**(6111): p. 1193-1196.
6. Saito, Y., et al., *Metallic ground state in an ion-gated two-dimensional superconductor.* Science, 2015. **350**(6259): p. 409-413.
7. Lu, J.M., et al., *Evidence for two-dimensional Ising superconductivity in gated MoS2.* Science, 2015. **350**(6266): p. 1353-1357.
8. Saito, Y., et al., *Superconductivity protected by spin-valley locking in ion-gated MoS2.* Nature Physics, 2016. **12**(2): p. 144-149.
9. Xi, X., et al., *Ising pairing in superconducting NbSe2 atomic layers.* Nature Physics, 2016. **12**(2): p. 139-143.
10. Saito, Y., T. Nojima, and Y. Iwasa, *Quantum phase transitions in highly crystalline two-dimensional superconductors.* Nature Communications, 2018. **9**(1): p. 778.
11. Xing, Y., et al., *Ising Superconductivity and Quantum Phase Transition in Macro-Size Monolayer NbSe2.* Nano Letters, 2017. **17**(11): p. 6802-6807.
12. Xing, Y., et al., *Quantum Griffiths singularity of superconductor-metal transition in Ga thin films.* Science, 2015. **350**(6260): p. 542-545.
13. Liu, Y., et al., *Anomalous quantum Griffiths singularity in ultrathin crystalline lead films.* Nature Communications, 2019. **10**(1): p. 3633.
14. Liu, Y., et al., *Interface-Induced Zeeman-Protected Superconductivity in Ultrathin Crystalline Lead Films.* Physical Review X, 2018. **8**(2): p. 021002.
15. Yang, C., et al., *Intermediate bosonic metallic state in the superconductor-insulator transition.* Science, 2019. **366**(6472): p. 1505-1509.
16. Saito, Y., T. Nojima, and Y. Iwasa, *Highly crystalline 2D superconductors.* Nature Reviews Materials, 2016. **2**: p. 16094.
17. Friend, R.H. and A.D. Yoffe, *Electronic properties of intercalation complexes of the transition metal dichalcogenides.* Advances in Physics, 1987. **36**(1): p. 1-94.
18. Woollam, J.A. and R.B. Somoano, *Physics and chemistry of MoS2 intercalation compounds.* Materials Science and Engineering, 1977. **31**: p. 289-295.
19. Somoano, R.B. and A. Rembaum, *Superconductivity in Intercalated Molybdenum Disulfide.* Physical Review Letters, 1971. **27**(7): p. 402-404.
20. Somoano, R.B., V. Hadek, and A. Rembaum, *Alkali metal intercalates of molybdenum disulfide.* The Journal of Chemical Physics, 1973. **58**: p. 697.
21. Eda, G., et al., *Coherent Atomic and Electronic Heterostructures of Single-Layer MoS2.* ACS Nano, 2012. **6**(8): p. 7311-7317.
22. Zhang, R., et al., *Superconductivity in Potassium-Doped Metallic Polymorphs of MoS2.* Nano Letters, 2016. **16**(1): p. 629-636.
23. Tan, S.J.R., et al., *Chemical Stabilization of 1T′ Phase Transition Metal Dichalcogenides with Giant Optical Kerr Nonlinearity.* Journal of the American Chemical Society, 2017. **139**(6): p. 2504-2511.
24. Graybeal, J.M. and M.R. Beasley, *Localization and interaction effects in ultrathin amorphous superconducting films.* Physical Review B, 1984. **29**(7): p. 4167-4169.

25. Ng, H.K., et al., *Effects Of Structural Phase Transition On Thermoelectric Performance in Lithium-Intercalated Molybdenum Disulfide (LixMoS2).* ACS Applied Materials & Interfaces, 2019. **11**(13): p. 12184-12189.
26. Steiner, M.A., N.P. Breznay, and A. Kapitulnik, *Approach to a superconductor-to-Bose-insulator transition in disordered films.* Physical Review B, 2008. **77**(21): p. 212501.
27. Werthamer, N.R., E. Helfand, and P.C. Hohenberg, *Temperature and Purity Dependence of the Superconducting Critical Field, Hc. III. Electron Spin and Spin-Orbit Effects.* Physical Review, 1966. **147**(1): p. 295-302.
28. Maki, K., *Effect of Pauli Paramagnetism on Magnetic Properties of High-Field Superconductors.* Physical Review, 1966. **148**(1): p. 362-369.
29. Tinkham, M., *Introduction to Superconductivity*. second ed. 2015: Dover Publications, Mineola, NY.
30. Tedrow, P.M. and R. Meservey, *Critical magnetic field of very thin superconducting aluminum films.* Physical Review B, 1982. **25**(1): p. 171-178.
31. Tinkham, M., *Effect of Fluxoid Quantization on Transitions of Superconducting Films.* Physical Review, 1963. **129**(6): p. 2413-2422.
32. Kim, M., et al., *Intrinsic spin-orbit coupling in superconducting d-doped SrTiO3 heterostructures.* Physical Review B, 2012. **86**(8): p. 085121.
33. Ueno, K., et al., *Effective thickness of two-dimensional superconductivity in a tunable triangular quantum well of SrTiO3.* Physical Review B, 2014. **89**(2): p. 020508.
34. Kosterlitz, J.M. and D.J. Thouless, *Ordering, metastability and phase transitions in two-dimensional systems.* Journal of Physics C: Solid State Physics, 1973. **6**(7): p. 1181-1203.
35. Sharma, C.H., et al., *2D superconductivity and vortex dynamics in 1T-MoS2.* Communications Physics, 2018. **1**(1): p. 90.
36. Sondhi, S.L., et al., *Continuous quantum phase transitions.* Reviews of Modern Physics, 1997. **69**(1): p. 315-333.
37. Fisher, M.P.A., *Quantum phase transitions in disordered two-dimensional superconductors.* Physical Review Letters, 1990. **65**(7): p. 923-926.